Submarine Mudflows: Insights from Depth-Averaged Numerical Simulation

Lucas D. F. Lino[1], Tiago P. S. Lôbo[1], Adeildo S. R. Júnior[1]

[1]*Laboratory of Scientific Computing and Visualization, Federal University of Alagoas*
Av. Lourival Melo Mota, S/N, Tabuleiro do Martins, 57072-900, Maceió/AL, Brazil
lucaslino@lccv.ufal.br, tiago@lccv.ufal.br, ricardoaf@lccv.ufal.br, adramos@lccv.ufal.br

Abstract. Submarine mudflows, frequently triggered by underwater landslides, lead to substantial debris accumulation stretching over kilometers once the landslide subsides, posing significant risks to vital infrastructure and the potential for triggering tsunamis. As these events are challenging to measure directly, simulation becomes imperative. Furthermore, these simulations must accurately depict the intricate dynamics of mudflow sliding processes, often modeled as viscoplastic fluids, and effectively captured by rheological models like Herschel-Bulkley and Bingham. The potential nonlinearity inherent in the Herschel-Bulkley model adds to the complexity of predicting final runout distances. The governing equations, comprised of a set of partial differential equations, further compound this challenge, making their solution difficult. In this paper, we delve into the numerical simulation of mudflows using the Depth-Averaged Method (DAM), a technique that streamlines the governing equations by integrating the momentum and continuity equations over the depth dimension. The mud descends down a slope with a fixed angle of declination. Using a finite difference scheme to solve the governing equations, we validated our numerical model against experimental data of a Bingham mudflow, achieving good agreement. A sensitivity analysis was conducted by varying the temporal and spatial discretization in a submarine mudflow. Root Mean Squared Error (RMSE) computations demonstrated that finer discretization yields more accurate simulations, while coarser discretization increases errors. However, good results can still be achieved with a careful selection of both parameters.

Keywords: Submarine mudflows, Bingham model, Depth-Averaged Method

1 Introduction

Debris flow is one of the gravity-driven downslope processes that transport sediment onto the seabed [1]. Characterized by plastic rheology and steady flow dynamics, debris flow can occur in both subaerial and submarine environments. These flows can consist of various sediment sizes, including fine particles (muddy debris flows), coarser particles (sandy debris flows), or a combination of both [2].

Subaerial mudflows, often triggered by intense rainfall in mountainous regions, have the potential to dramatically reshape the landscape and inflict significant harm on wildlife and human communities in the surrounding areas [3]. Equally important are submarine muddy debris flows, which have the capacity to transport vast quantities of sediment, often amounting to thousands of cubic kilometers [4]. These submarine mudflows pose significant hazards, including the potential to trigger tsunamis and damage underwater infrastructure such as oil and gas pipelines and subsea internet cables [5].

Accurate understanding and prediction of the physical processes of both submarine and subaerial mudflows are crucial for mitigating the risks associated with geohazard-induced destruction. However, monitoring and measuring these mudflows present significant challenges due to their brief duration, infrequent occurrence and unpredictable nature. To address these challenges, controlled laboratory environments are used to study these complex flow phenomena [5, 6]. In parallel, researchers have developed simulations of submarine and subaerial muddy debris flow dynamics by leveraging data from field investigations and laboratory experiments. These efforts involve the application of analytical models [3, 7] and numerical models [8–11].

Numerical simulations of mudflows require methods that can accurately predict runout distances, morphology, and account for plastic rheological models. Most simulations use the Bingham and Herschel-Bulkley models [3, 7, 12]. The possible nonlinearity of the plastic model adds complexity to solving the governing partial differential equations, making the selection of an appropriate numerical method challenging.

Researchers frequently use the Depth-Averaged Method (DAM) for simulating mudflow movement with the Herschel-Bulkley and Bingham models due to its efficiency in predicting runout distances and final debris flow morphology while minimizing computational effort. The DAM approach relies on boundary layer approximations, assuming that the mud thickness is small compared to its length [13]. It simplifies the governing equations by integrating the momentum and continuity equations over the depth dimension, a technique formerly known as von Kármán's momentum integral method. This integration simplifies the problem to either a one-dimensional computation (in the case of 2D simulations) or a two-dimensional computation (for 3D simulations), enhancing the computational efficiency of the DAM.

Despite its efficiency, the DAM can still introduce errors due to the inherent complexity of debris flow dynamics, especially in submarine environments. Simplifications in the governing equations may lead to inaccuracies depending on the specific simulation conditions and rheological parameters used.

In this paper, we applied the Depth-Averaged Method, solved with a finite difference scheme, with the Bingham model to simulate submarine mudflows. We began by validating our numerical results against experimental data from Ghahramani-Wright. Following this, we performed a sensitivity analysis based on Huang and García's analytical model of a hypothetical submarine slide. This analysis examined how variations in the simulation parameters - specifically the spatial and temporal discretization of the model - affect the final runout distance and morphology of the mudflows.

2 Depth-Averaged Method (DAM)

Presenting the formulation of DAM using the Herschel-Bulkley model offers greater convenience and flexibility, as it includes the Bingham model as a special case. Moreover, it accounts for shear thinning, where viscosity decreases gradually with increasing shear rate, a behavior commonly observed in many mudflows experiments [7]. In simple shear, the stress-strain relationship for a Herschel-Bulkley fluid in laminar flow is:

$$\mu_n \left|\frac{\partial u}{\partial y}\right|^n \operatorname{sgn}\left(\frac{\partial u}{\partial y}\right) = \begin{cases} 0 & \text{if } |\tau| < \tau_y \\ \tau - \tau_y \operatorname{sgn}\left(\frac{\partial u}{\partial y}\right) & \text{if } |\tau| \geq \tau_y \end{cases}, \tag{1}$$

in which, τ is the shear stress, τ_y is the yield stress, μ_n indicates the dynamic viscosity of dimension $\left[\frac{M\,T^{(n-2)}}{L}\right]$ and the flow index n varies from 0 to 1 [7]. The strain rate is defined as $\partial u/\partial y$, where u is the longitudinal velocity (parallel to the bed). The Bingham plastic fluid equation is obtained by considering $n = 1$ in equation eq. (1).

We consider a two-dimensional flow where the flow depth is relatively small compared to the downslope flow length, and the flow characteristics vary gradually along the longitudinal direction. These conditions are consistent with boundary layer approximations. Additionally, the analysis assumes equilibrium conditions, meaning that no erosion or deposition takes place.

The coordinate system is defined with the x-axis oriented along the downslope flow direction and the y-axis perpendicular to the bed plane, which is inclined at an angle θ relative to the horizontal. The longitudinal and transversal velocity components are denoted by u and v, respectively; p represents the pressure; and $h = h_s + h_p$ denotes the total flow depth normal to the bed, as illustrated in Fig. 1.

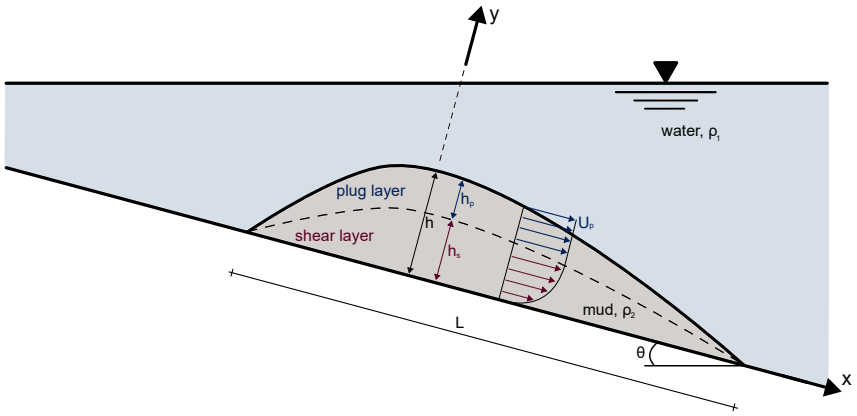

Figure 1. Illustration of a two-dimensional submarine mudflow descending a slope with angle θ. The diagram highlights two distinct zones: the shear region, where velocity transitions from 0 to U_p, and the plug region, where the velocity remains constant at U_p.

As depicted in Fig. 1, using a Herschel-Bulkley rheological model (and consequently for the Bingham model) results in two distinct zones: a shear flow region, where the shear stress exceeds the yield stress $\tau \geq \tau_y$ and the longitudinal velocity u varies from 0 to the plug velocity U_p, along the direction perpendicular to the bed ($0 \leq y \leq h_s$); and a plug flow region, where the shear stress is below the yield stress ($\tau < \tau_y$) and the velocity $u = U_p$ is uniform ($h_s \leq y \leq h_s + h_p$).

The governing equations, based on the previously stated boundary layer approximation assumptions, are as follows [14]:

$$\begin{aligned} \rho_2 \left(\frac{\partial u}{\partial t} + u \frac{\partial u}{\partial x} + v \frac{\partial u}{\partial y} \right) &= -\frac{\partial p}{\partial x} + \rho_2 g \sin\theta + \frac{1}{\rho} \frac{\partial \tau}{\partial y} \\ 0 &= -\frac{\partial p}{\partial y} - \rho_2 g \cos\theta \qquad , \\ \frac{\partial u}{\partial x} + \frac{\partial v}{\partial y} &= 0 \end{aligned} \tag{2}$$

where, ρ_2 is the bulk density of the mud and g is the gravity acceleration. For the case of an unsteady and nonuniform (velocity varying with space and time), laminar flow, the y-momentum term from eq. (2) and the water pressure boundary condition, $p\left(x,\, y = h\right) = \rho_1 g h_w \cos\theta$, are used to approximate the pressure as hydrostatic:

$$p\left(x,\, y,\, t\right) = \rho_2 g \left(h_s\left(x,\, t\right) + h_p\left(x,\, t\right) - y\right) \cos\theta + \rho_1 g h_w\left(x,\, t\right) \cos\theta, \tag{3}$$

in which ρ_1 is the density of the water and h_w is the water depth. By incorporating the pressure term from eq. (3) into the x-momentum term of eq. (2), we obtain the x-axis momentum equation for a submarine landslide [14]:

$$\frac{\partial u}{\partial t} + u \frac{\partial u}{\partial x} + v \frac{\partial u}{\partial y} = -g' \frac{\partial \left(h_s + h_p\right)}{\partial x} \cos\theta + g' \sin\theta + \frac{1}{\rho_2} \frac{\partial \tau}{\partial y}, \tag{4}$$

where $g' = g \cdot \left(\rho_2 - \rho_1\right) / \rho_2$. Note that all of the equations reduce to those for subaerial flows if $\rho_1 = 0$.

Rather than solving the boundary-value problem directly, we begin by assuming a plausible velocity profile for the longitudinal velocity across the mud depth. For this, we selected the profile from the steady, uniform flow case, which satisfies all boundary conditions. Using this assumed profile, we integrate the momentum equation over the depth. This approach, known as von Kármán's momentum integral method in boundary layer theory, is commonly employed due to the complexity of obtaining exact solutions, particularly in scenarios involving more than simple steady flow over a flat bed with zero inclination.

Integrating the momentum equations across the mud depth results in differential equations for the shear flow region, the plug flow region, and the entire mud depth, with the unknowns U_p and h. The differential equations for the plug flow region and the entire flow region are presented below:

$$\begin{aligned} \frac{\partial U_p}{\partial t} + \frac{\partial}{\partial x} \left(\frac{U_p^2}{2} + g' h \cos\theta \right) &= g' \sin\theta - \frac{\tau_y \,\mathrm{sgn}\left(U_p\right)}{\rho \left(h - h_s\right)} \\ \frac{\partial}{\partial t} \left[U_p \left(h_p + \alpha_1 h_s\right)\right] + \frac{\partial}{\partial x} \left[U_p^2 \left(h_p + \alpha_2 h_s\right)\right] &= h g' \left(\sin\theta - \cos\theta \frac{\partial h}{\partial x} \right) - \frac{\tau_b}{\rho} \end{aligned} \tag{5}$$

The parameters α in eq. (5) are defined as follows:

$$\alpha_1 U_p h_s = \int_0^{h_s} u \,\mathrm{d}y = \frac{n+1}{2n+1} \quad \text{and} \quad \alpha_2 U_p^2 h_s = \int_0^{h_s} u^2 \,\mathrm{d}y = \frac{2\left(n+1\right)^2}{\left(2n+1\right)\left(3n+2\right)} \tag{6}$$

Based on the solutions provided by Savage and Hutter and Imran et al., we solve the preceding equations using a finite difference scheme by discretizing the mud into multiple column elements. Here, we present the forward difference method with first-order accuracy for the governing equations of the Herschel-Bulkley model. These equations can be adapted to the Bingham model by selecting appropriate values for α_1 and α_2. Using the material derivative definition [16] and applying the forward difference, we determine the plug velocity U_p and the averaged velocity U for a column element at time step $t + \Delta t$ as follows:

$$
\begin{aligned}
U_p^{t+\Delta t} &= U_p^t + \Delta t \left[(U - U_p) \frac{\partial U_p}{\partial x} - g' \cos\theta \frac{\partial h}{\partial x} + g' \sin\theta - \frac{\tau_y \operatorname{sgn}(U_p)}{\rho (h - h_s)} \right] \\
U^{t+\Delta t} &= U^t + \left\{ \frac{1}{h} \frac{\partial}{\partial x} \left(U^2 h - \frac{\alpha_1 - \alpha_2}{\alpha_1 - 1} U_p^2 h - \frac{\alpha_2 - 1}{\alpha_1 - 1} U_p U h \right) \right. \\
&\quad \left. + g' \left(\sin\theta - \cos\theta \frac{\partial h}{\partial x} \right) - \frac{1}{h\rho} \left(\tau_y + \mu_n \left| \frac{n+1}{n} \frac{U_p}{h_s} \right|^n \right) \operatorname{sgn}(U_p) \right\} \Delta t
\end{aligned} \tag{7}
$$

These equations provide solutions for the average velocity U and the plug velocity U_p, applicable to both Herschel-Bulkley and Bingham models. Finally, we want to highlight that a well-known application of the DAM is the BING software, developed by Imran et al. Initially programmed in Visual Basic, this software has since been expanded with various extensions [9, 10]. In this study, we have ported and customized BING to Python to better support our analysis.

3 Numerical Simulations

Observing submarine mudflows is challenging due to the location's inherent difficulties and the unpredictable nature of the events. Therefore, we initially validated our numerical adapted model by following the approach of Huang and García (1997) and Imran et al., using the experimental data from Ghahramani-Wright's study of a subaerial Bingham mudflow. In this study, mudflows were analyzed in a rectangular glass flume with an upstream reservoir measuring 1.8 meters in length. The reservoir was filled with bentonite slurry, and an instantaneous dam break was simulated by releasing a vertical sliding gate at its downstream end. One of the experimental simulations was conducted under the following conditions: initial mud length L of $1.8\,\mathrm{m}$, initial mud height h of $0.3\,\mathrm{m}$, yield strength τ_y of $42.5\,\mathrm{Pa}$, dynamic viscosity μ of $0.22\,\mathrm{Pa/s}$, Herschel-Bulkley exponent $n = 1$ (representing a Bingham fluid), ambient fluid density ρ_1 of $1\ \mathrm{kg/m^3}$, and mud density ρ_2 of $1073\ \mathrm{kg/m^3}$. The bed profile had a constant slope of 3.43 degrees. The initial debris length of $1.8\,\mathrm{m}$ was divided into 20 column cells, each measuring $0.09\,\mathrm{m}$, and a time step of $\Delta t = 6.88 \cdot 10^{-5}$ seconds was used.

Figure 2(a) presents the surface profiles at $t = 4.1\,\mathrm{s}$, comparing experimental measurements with simulations from both BING by Imran et al. and our adapted model. As observed, our simulation aligns closely with the laboratory measurements and matches exactly with the results from BING, as expected. However, the final runout distance is slightly greater than what was measured. Additionally, the mudflow is obstructed from moving left due to the back wall of the reservoir in the laboratory setup. Nonetheless, the simulation accurately represents the flow depth, which is approximately $0.05\,\mathrm{m}$.

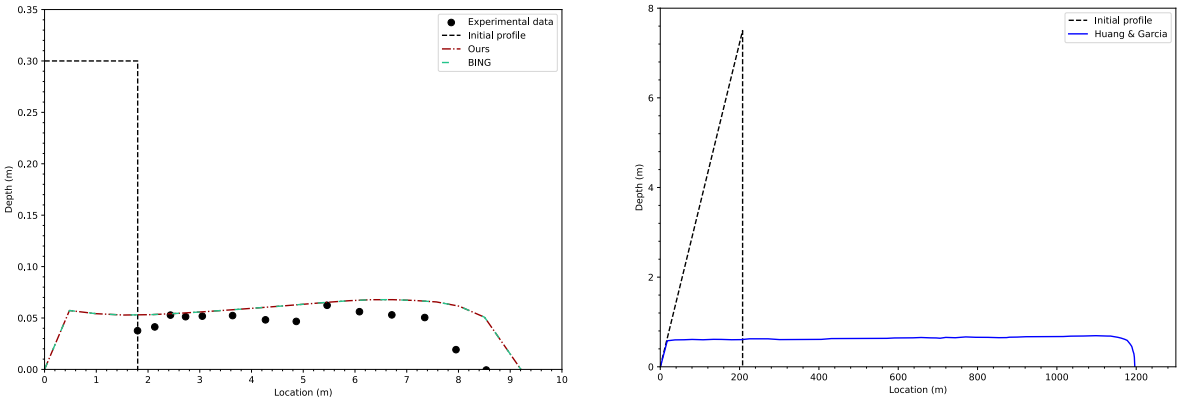

(a) Comparison between experimental data by Ghahramani-Wright, BING simulation (cyan line) and our simulation (red line) at $t = 4.1\,\mathrm{s}$.

(b) Initial profile of submarine mudflow alongside the final results from Huang and García's analytical model at $t = 2.5\,\mathrm{min}$.

Figure 2. Comparison of our simulation with experimental data and BING simulation results at $t = 4.1\,\mathrm{s}$ (left), and the initial profile and final results of submarine mudflow based on Huang and García's analytical model (right).

To study submarine mudflows, we based our research on Huang and García's (1999) analytical model results of a hypothetical submarine mudflow, which used parameters derived from field observations of subaerial mudflow

properties described by O'Brien and Julien (Fig. 2(b)). We focused on examining the simulation parameters and conducted a sensitivity analysis to compare our results with their findings. The initial mud mass distribution is triangular, with a horizontal base and a vertical side oriented downslope, as illustrated in Fig. 2(b).

The simulation parameters are as follows: the initial mud height is $7.25\,\mathrm{m}$ with an initial length of $207.6\,\mathrm{m}$, a mud density of $\rho_2 = 2000\,\mathrm{kg/m^3}$, and a water density of $\rho_1 = 1000\,\mathrm{kg/m^3}$. The yield stress is $\tau_y = 200\,\mathrm{Pa}$, the dynamic viscosity is $\mu = 10\,\mathrm{Pa/s}$ and the flow index $n = 1$ to consider the Bingham model. The bed slope angle is always 2 degrees with respect to the horizontal, and the final simulation morphology is analyzed at $t = 2.5\,\mathrm{min}$ (Fig. 2(b)). We varied the spatial discretization dx of the column elements of the mud mass from $0.5\,\mathrm{m}$ to $10.5\,\mathrm{m}$ in increments of $1\,\mathrm{m}$, and the temporal discretization, time step dt, of the simulation from $0.0005\,\mathrm{s}$ to $0.105\,\mathrm{s}$ in increments of $0.0010\,\mathrm{s}$, resulting in a total of 121 simulations generated by the combination of these parameters.

For each simulation, we compared the final runout distance and morphology results with those of Huang and García. We calculated the absolute error for each node by determining the minimum distance to the reference curve and then computed the Root Mean Squared Error (RMSE) for each of the 121 simulations.

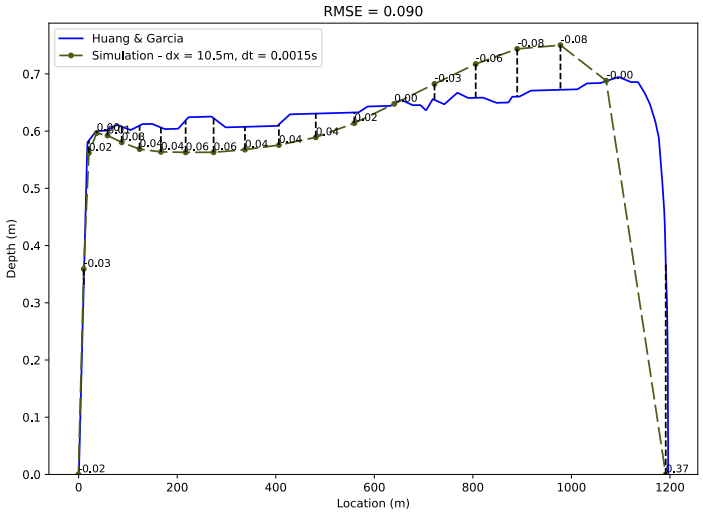

Figure 3. Details of computation of the Root Mean Squared Error (RMSE) for the simulation with $dx = 10.5\,\mathrm{m}$ and $dt = 0.0015\,\mathrm{s}$, resulting in a RMSE of 0.090 at $t = 2.5\,\mathrm{min}$.

Figure 3 illustrates the computation of the RMSE for the simulation with $dx = 10.5\,\mathrm{m}$ and $dt = 0.0015\,\mathrm{s}$. It shows the absolute error, representing the distance to the curve, computed for all 21 nodes, which resulted in an RMSE value of 0.090 for this simulation. Using this approach, we first conducted an analysis of the influence of spatial discretization on the final results at $t = 2.5\,\mathrm{min}$. By fixing the time step at $dt = 0.0005\,\mathrm{s}$ and varying dx, we were able to investigate how different levels of spatial resolution affected the accuracy of our simulation. The results of this investigation are presented in Fig. 4(a), highlighting the relationship between discretization and the resultant RMSE values.

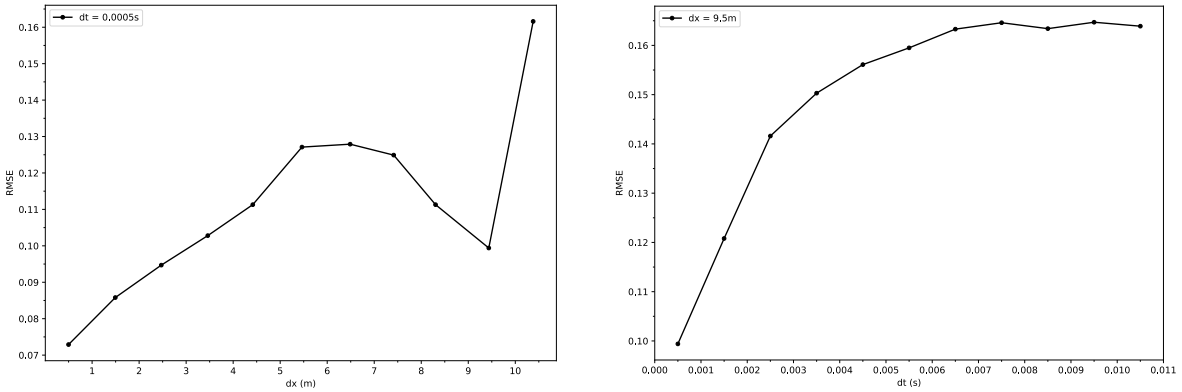

(a) RMSE values for $dt = 0.0005\,\mathrm{s}$ and varying dx.

(b) RMSE values for $dx = 9.5\,\mathrm{m}$ and varying dt.

Figure 4. Impact of spatial and temporal discretization on RMSE values.

In Fig. 4(a), we can observe a general trend where smaller spatial discretization dx values correspond to lower RMSE values. Specifically, from $dx = 0.5\,\mathrm{m}$ to $dx = 5.5\,\mathrm{m}$, there is a noticeable increase in RMSE. However, beyond this point, we notice an unexpected reduction in RMSE, before observing a significant increase again at $dx = 10.5\,\mathrm{m}$, where the RMSE value reaches 0.162. This indicates that the relationship between spatial discretization and RMSE can be influenced by other factors in the simulation setup. Continuing with this approach, we fixed $dx = 9.5\,\mathrm{m}$ and varied the time step dt. The results of this analysis are presented in Fig. 4(b), which show that smaller dt values correspond to lower RMSE values. However, after reaching a certain dt, the error stabilizes, despite being already high. This suggests that while finer temporal resolution improves accuracy initially, beyond a certain point, further increasing dt does not drastically increase the error. Thus, it is essential to find a balance where dt is small enough to maintain accuracy but not unnecessarily fine, ensuring computational efficiency. By comparing the two results in Fig. 4, we can better understand the trade-offs between spatial and temporal resolution in optimizing simulation accuracy.

A comprehensive investigation was conducted, and the RMSE values for all 121 simulations are presented. However, it is important to note that some simulations did not complete successfully, particularly those with $dx = 0.5\,\mathrm{m}$ and larger time steps. Additionally, some simulations produced completely erroneous results, resulting in high RMSE values. This is illustrated in Fig. 5(a), where a heatmap shows the RMSE values, with dx on the x-axis and dt on the y-axis. The presence of strong red spots indicates simulations that failed, leading to exceptionally huge RMSE values.

In most cases, the solution remains stable if the time step is sufficiently small. Stability can be ensured by applying the Courant–Friedrichs–Lewy (CFL) condition, $\mathrm{CFL} = a \cdot dt/dx \geq 1$, where a is the wave speed. We adapted the CFL condition and computed a disarable dt using the generalized formula $k\sqrt{dx/g}$, with $k = 0.005$, dx being the initial grid size, and g representing the gravitational acceleration. This approach, similar to that used by Imran et al., is employed because calculating wave speed directly for submarine debris flows is challenging due to varying conditions and complex interactions. This generalized form based on g and dx provides a practical and reliable stability condition, and our tests confirmed that $k = 0.005$ is a valid value.

In Fig. 5(a), we also computed those potential stable dt using the previously mentioned formula and overlaid this with the heatmap. A clear pattern emerges: above the line representing stable dts, we observe strong red spots, indicating that instability occurred due to excessively large time steps. This visualization highlights the critical importance of adhering to the stability condition to prevent simulation errors.

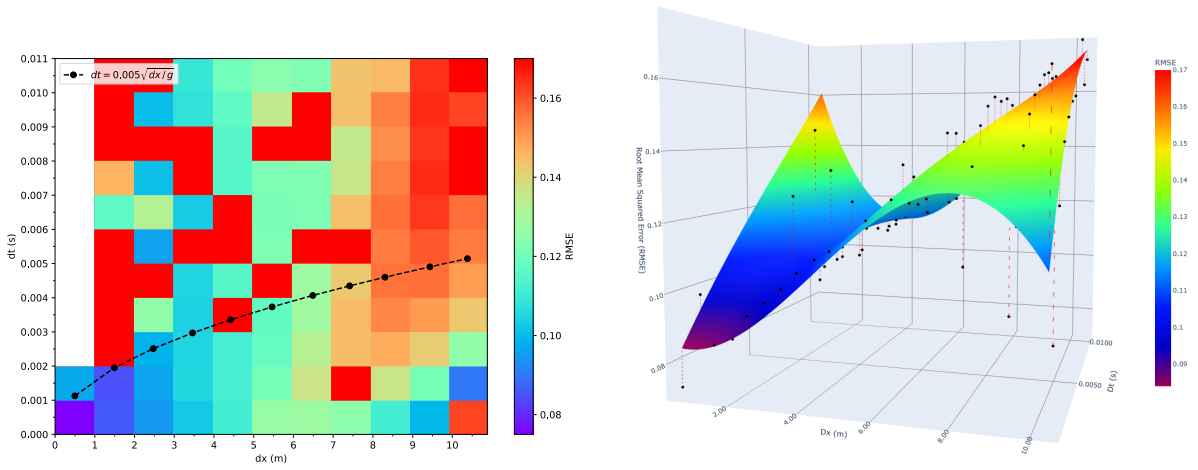

(a) Heatmap of RMSE values for all simulations, with RMSE represented by color. Desirable stable time steps computed with the adapted CFL condition are also indicated.

(b) Regression surface showing the relationship between dx, dt, and RMSE. The distances between simulation points and the surface are highlighted.

Figure 5. Analysis of RMSE values across different spatial and temporal discretizations.

The unstable cases were removed to allow for a clearer analysis of RMSE trends through a surface regression in a 3D graph, where RMSE is the z-axis (Fig. 5(b)). The surface was approximated by a third-degree polynomial, resulting in an R^2 value of 0.81, with the residuals well-distributed along the zero line of the adjusted residuals chart. This result supports our previous discussions: large (dx, dt) values lead to higher errors, and smaller (dx, dt) values lead to lower errors, with an intermediary region exhibiting reasonable RMSE values. Therefore, it is crucial to carefully consider the trade-offs between accuracy and computational cost when selecting these parameters.

4 Conclusions

Our study validated a numerical model using experimental data and investigated the effects of spatial and temporal discretization on the accuracy of submarine mudflow simulations through the computation of RMSE. We found that finer discretizations generally yield lower RMSE values, while larger ones increase errors. Many simulations failed because the CFL condition was not met, highlighting the importance of adhering to this stability criterion. These findings emphasize the need to balance the choice of dx and dt to achieve acceptable accuracy. Future work should integrate computational cost into the selection of dx and dt, considering the trade-offs between accuracy and efficiency.

Acknowledgements. The authors would like to express their gratitude to the Laboratory of Scientific Computing and Visualization (LCCV) for providing the computational resources and support necessary for this study. We also extend our thanks to the researchers involved in the MPM project for their valuable insights and contributions.

Authorship statement. The authors hereby confirm that they are the sole liable persons responsible for the authorship of this work, and that all material that has been herein included as part of the present paper is either the property (and authorship) of the authors, or has the permission of the owners to be included here.

References

[1] G. Shanmugam. Chapter 2 – Mass transport: Slides, slumps, and debris flows. *Mass transport, gravity flows, and bottom currents*, vol. 1, pp. 7–88, 2021.
[2] X. Qian, J. Xu, H. S. Das, D. Wang, and Y. Bai. Improved Modeling of Subaerial and Subaqueous Muddy Debris Flows. *Journal of Hydraulic Engineering*, vol. 146, n. 7, 2020.
[3] X. Huang and M. H. García. A perturbation solution for bingham-plastic mudflows. *Journal of hydraulic Engineering*, vol. 123, n. 11, pp. 986–994, 1997.
[4] J. Kim, F. Løvholt, D. Issler, and C. F. Forsberg. Landslide material control on tsunami genesis—the storegga slide and tsunami (8,100 years bp). *Journal of Geophysical Research: Oceans*, vol. 124, n. 6, pp. 3607–3627, 2019.
[5] D. Mohrig, C. Ellis, G. Parker, K. X. Whipple, and M. Hondzo. Hydroplaning of subaqueous debris flows. *Geological Society of America Bulletin*, vol. 110, n. 3, pp. 387–394, 1998.
[6] V. Ghahramani-Wright. *Laboratory and Numerical Study of Mud and Debris Flow*. PhD thesis, University of California, Davis, 1987.
[7] X. Huang and M. H. García. A Herschel–Bulkley model for mud flow down a slope. *Journal of Fluid Mechanics*, vol. 374, 1998.
[8] J. Imran, P. Harff, and G. Parker. A numerical model of submarine debris flow with graphical user interface. *Computers & Geosciences*, vol. 27, n. 6, 2001.
[9] F. De Blasio, A. Elverhøi, D. Issler, C. Harbitz, P. Bryn, and R. Lien. Flow models of natural debris flows originating from overconsolidated clay materials. *Marine Geology*, vol. 213, n. 1-4, 2004.
[10] Y. Dong, D. Wang, and L. Cui. Assessment of depth-averaged method in analysing runout of submarine landslide. *Landslides*, vol. 17, pp. 543–555, 2020.
[11] H. Vicari, Q. A. Tran, S. Nordal, and V. Thakur. Mpm modelling of debris flow entrainment and interaction with an upstream flexible barrier. *Landslides*, vol. 19, n. 9, pp. 2101–2115, 2022.
[12] L. Jiang and P. H. LeBlond. Numerical modeling of an underwater Bingham plastic mudslide and the waves which it generates. *Journal of Geophysical Research: Oceans*, vol. 98, n. C6, 1993.
[13] G. K. Batchelor. *An introduction to fluid dynamics*. Cambridge university press, 2000.
[14] X. Huang and M. H. García. Modeling of non-hydroplaning mudflows on continental slopes. *Marine Geology*, vol. 154, n. 1-4, 1999.
[15] S. B. Savage and K. Hutter. The motion of a finite mass of granular material down a rough incline. *Journal of fluid mechanics*, vol. 199, pp. 177–215, 1989.
[16] W. M. Lai, D. Rubin, and E. Krempl. *Introduction to continuum mechanics*. Butterworth-Heinemann, 2009.
[17] J. S. O'Brien and P. Y. Julien. Laboratory analysis of mudflow properties. *Journal of hydraulic engineering*, vol. 114, n. 8, pp. 877–887, 1988.